FEMS Microbiology Ecology, 91, 2015, fiv068

doi: 10.1093/femsec/fiv068
Advance Access Publication Date: 22 June 2015
Research Article

RESEARCH ARTICLE

Microzooplankton community associated with phytoplankton blooms in the naturally iron-fertilized Kerguelen area (Southern Ocean)

Urania Christaki*, Clément Georges, Savvas Genitsaris and Sébastien Monchy

INSU-CNRS, UMR 8187 LOG, Laboratory of Oceanology and Geosciences, University of Littoral - Opal Coast, ULCO 32 avenue Foch, F-62930 Wimereux, France

*Corresponding author: INSU-CNRS, UMR 8187 LOG, Laboratory of Oceanology and Geosciences, University of Littoral - Opal Coast, ULCO 32 avenue Foch, F-62930 Wimereux, France. Tel: +33 321 99 64 35; E-mail: Urania.Christaki@univ-littoral.fr

One sentence summary: The aim of this study was to improve our knowledge of the spatial and temporal variation of the understudied microzooplankton communities associated with massive diatom blooms in the Southern Ocean.

Editor: Gary King

Downloaded from http://femsec.oxfordjournals.org/ by guest on October 6, 2016

ABSTRACT

The spatial and temporal community composition of microzooplankton (dinoflagellates and ciliates) was assessed in the Kerguelen area (Southern Ocean) during the KEOPS2 cruise in early spring (October–November) 2011. This naturally iron-fertilized region was characterized by a complex mesoscale circulation resulting in a patchy distribution of phytoplankton blooms. Collectively, 97 morphospecies of dinoflagellates and ciliates belonging to 41 genera were identified by microscopy, and 202 Alveolata-related OTUs (operational taxonomical units) were retrieved with tag-pyrosequencing. Microscopy and pyrosequencing data were in accordance, in that diatom-consuming dinoflagellates were the most enhanced taxa in the blooms. Dinoflagellates also showed significant positive relationships with phytoplankton pigments, while no major differences were found in the ciliate abundances inside and outside the blooms. Cluster analysis showed clear differences in the phytoplankton and microzooplankton community structures between the iron-fertilized and HNLC (high nutrient low chlorophyll) waters, and between the blooms, concerning their location and the fertilization mechanisms. These results were combined with the rates of primary production and mesozooplankton consumption determined for the study area. The potential role of dinoflagellates and ciliates as phytoplankton consumers and as prey for mesozooplankton was then evaluated. Overall, heterotrophic dinoflagellates were probably the most important group of phytoplankton grazers, and a potential food source for copepods.

Keywords: dinoflagellates; ciliates; natural iron fertilization; Southern Ocean

INTRODUCTION

In addition to being the world's largest HNLC (high nutrient low chlorophyll) area, the Southern Ocean plays a major role in the biological uptake and sequestration of atmospheric CO_2; this has major climatic implications (e.g. Takahashi *et al.* 2002). It is now well documented that iron limits primary production in the HNLC regions, resulting in a large stock of unused major inorganic nutrients (e.g. Martin and Fitzwater 1990). Although the Southern Ocean is considered an HNLC area, massive and recurrent blooms are observed over and eastward of the Kerguelen

Received: 7 April 2015; **Accepted:** 14 June 2015
© FEMS 2015. All rights reserved. For permissions, please e-mail: journals.permissions@oup.com

plateau. The KEOPS1 cruise in summer 2005 demonstrated that the phytoplankton blooms were sustained by iron supply from iron-rich deep waters below, representing natural iron fertilization (Blain *et al.* 2007). Natural iron fertilization differs from artificial fertilizations in that major nutrients are supplied concomitantly with iron (Blain *et al.* 2007; Blain, Quéguiner and Trull 2008). The offshore waters east of Kerguelen Island represent an intense mixing zone that consists of several mesoscale eddies. Vertical transport and entrainment by deep waters are the main mechanisms of iron fertilization (Park *et al.* 2014; d'Ovidio *et al.* 2015), causing production rates which fall into some of the highest measured in the Southern Ocean (Cavagna *et al.* 2014). This environmental background provided the sampling of phytoplankton blooms at different stages and under varying hydrographic conditions, with large variation in local values of carbon production and export (Planchon *et al.* 2014; Christaki *et al.* 2014).

A pronounced shift to larger phytoplankton cells, in particular diatoms, has been generally observed during natural (Blain *et al.* 2007; Pollard *et al.* 2009; Quéguiner 2013; Lasbleiz *et al.* 2014) or artificial (Boyd *et al.* 2007; Smetacek *et al.* 2012) iron fertilization. The variations of the phytoplankton community are expected to correspond to the changes in the grazer communities regarding herbivorous protists (e.g. Grattepanche *et al.* 2011a, 2011b). Dinoflagellate and ciliate clades belonging to Alveolata are extremely well represented in all marine ecosystems. Phagotrophic dinoflagellates and ciliates play a key role in carbon transfer as primary consumers of pico- and nanoplankton (e.g Pierce and Turner 1992), microphytoplankton, and as a food resource for higher trophic levels (e.g. Stoecker and Capuzzo 1990; reviewed in Sherr and Sherr 2007; Montagnes *et al.* 2010). Additionally, parasitic alveolate forms belonging to the novel clade of marine alveolates (MALVs)—that have strong affinities for the dinoflagellates—appear in virtually all the molecular marine surveys (e.g López-Garcia *et al.* 2001; Díez, Pedrós-Alió and Massana 2001; Moon-van der Staay, Watcher and Vaulot 2001; Massana and Pedrós-Alió 2008). Few studies provide any information regarding microzooplankton during iron fertilization. Those that do have suggested an increase in the abundance of ciliates and dinoflagellates in the iron-fertilized induced blooms and their significant role as potential phytoplankton grazers (e.g. IronEx-II, Landry *et al.* 2000; SOIREE, Hall and Safi 2001; EisenEx, Henjes *et al.* 2007; SEEDS, Saito *et al.* 2005; KEOPS1, Brussaard *et al.* 2008; Christaki *et al.* 2008).

The KEOPS2 cruise investigated a large panel of diverse natural iron-fertilized stations at early bloom stages (October–November 2011) in the surrounding area of the Kerguelen plateau. As these diatom-dominated phytoplankton blooms are responsible for a major carbon sink in this area, the aim of this study was to understand better the spatial and temporal variation of the understudied microzooplankton communities associated with them. The hypothesis was that the communities would differ spatially and temporally in the natural iron-fertilized blooms and the HNLC waters in relation to the phytoplankton community structure and biomass. This was accomplished with microscopy at all sampled depths at each station, and complemented with Alveolata data from 454-pyrosequencing in the ML (mixed layer) of selected stations.

Finally, the potential role of dinoflagellates and ciliates as phytoplankton consumers, and as prey for mesozooplankton, was evaluated based on rates of primary production and mesozooplankton consumption.

MATERIALS AND METHODS

Sampling

The present study was carried out during the KEOPS2 cruise from 15 October to 20 November 2011. Stations were sampled in distinct zones, covering different bloom patterns: (a) on the shallow plateau constrained by the bathymetry, coinciding with a site studied during the KEOPS1 cruise, station A3 was sampled twice over a 27-day period (Fig. 1a and b; Table 1); (b) south of the polar front, based on the trajectories of two surface drifters, the 'E' stations E-1, E-3 and E-5 were sampled in a quasi-Lagrangian manner within a complex meander (Fig. 1a and b); (c) north of the polar front (station F-L; Fig. 1a and b) in a zone of retroflection of the polar front and of eddies mixing between Antarctic and sub-Antarctic surface waters; and (d) south-west of the plateau, a reference HNLC non-bloom/non-Fe-fertilized station (Fig. 1a; Table 1). The hydrographic context of the study region is described in more detail in Park *et al.* (2014) and d'Ovidio *et al.* (2015) and basic parameters are provided in Table 1. All water samples were collected with 12 L Niskin bottles mounted on a rosette equipped with a CTDO Seabird SBE911-plus.

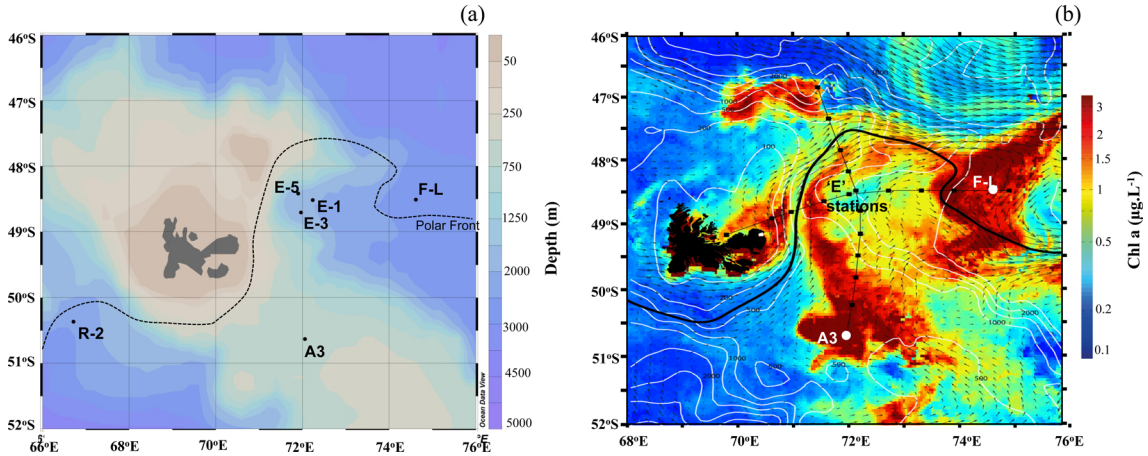

Figure 1. Bathymetry of the study area and location of the sampled stations (**a**), and (**b**) Chl *a* (color scale), surface velocity fields (arrows) and the polar front (PF, black line). The Chl *a*-rich stations: A3, on the Kerguelen plateau visited twice, F-L north of the polar front and 'E' stations sampled in a quasi-Lagrangian manner (E-1, E-3 and E-5) within a complex meander south of the polar front. The map is courtesy of Y. Park and colleagues. Note that the chlorophyll content represented on the map corresponds to the last week of the KEOPS2 cruise.

Downloaded from http://femsec.oxfordjournals.org/ by guest on October 6, 2016

Table 1. Brief description of the stations.

Stations	R-2	A3-1	A3-2	F-L	E-1	E-3	E-5
Date (2011)	26/10	20/10	16/11	7/11	30/10	4/11	19/11
Longitude East	66.7	72.1	72.1	74.8	72.2	72.0	71.9
Latitude North	−50.4	−50.6	−50.6	−48.6	−48.5	−48.7	−48.4
Depth (m)	2450	475	528	2690	2050	1923	1920
ML (m)	105 ± 15	168 ± 11	153 ± 15	38 ± 7	72 ± 38	38 ± 9	46 ± 13
Ze (m)	92	N/A	38	29	64	68	54
Chl *a* (μg L^{-1})[a]	0.28 ± 0.04	0.62 ± 0.17	2.03 ± 0.33	4.00 ± 1.58	0.94 ± 0.08	0.63 ± 0.08	1.15 ± 0.07
$NO_3^- + NO_2^-$ (μM)[b]	26.0 ± 0.2	29.7 ± 0.5	26.2 ± 0.4	20.5 ± 1.9	25.7 ± 0.5	26.2 ± 0.7	25.4 ± 0.2
PO_4^{3-} (μM)[b]	1.83 ± 0.03	2.00 ± 0.03	1.78 ± 0.03	1.06 ± 0.21	1.75 ± 0.05	1.79 ± 0.01	1.74 ± 0.04
$Si(OH)_4$ (μM)[c]	12.3 ± 0.3	23.7 ± 0.8	18.9 ± 0.5	7.7 ± 0.8	15.1 ± 0.4	15.2 ± 0.2	11.7 ± 0.2
dFe (nM)[d]	0.09 ± 0.01	0.37 ± 0.08	0.16 ± 0.03	0.26 ± 0.01	N/A	0.31 ± 0.07	0.10 ± 02

The depth of the mixed layer (ML) is based on a difference in sigma of 0.02 to the surface value. The mean ML (±SD) of all CTD casts performed during the occupation of the stations is given. The depth of the euphotic zone (Ze) corresponded to the depth of 1% of surface incident irradiance. For Chl *a* and major inorganic nutrients, mean values ± SD for the ML are also given. (N/A: not available).
[a]Lasbleiz *et al.* (2014), [b]Blain et al. (2015), [c]Closset *et al.* (2014), [d]Quéroué *et al.* (2015).

Molecular analysis

Water samples were collected at six stations (R-2, A3-2, F-L, E-1, E-3 and E-5) in the ML at 20 m. Five liters were subsequently filtered on 10, 3 and 0.6 μm, 47 mm nucleopore filters (Whatman, USA) using a serial filtration system at very low pressure (15 rpm). The filters were flash-frozen in liquid nitrogen and stored at −80°C. After pooling filters, DNA extraction was carried out using the MO BIO PowerWater DNA Isolation Kit (MO BIO Laboratories, Inc., Carlsbad, CA, USA), following the manufacturer's protocol. In order to obtain the pyrosequences, the methodology used in Georges *et al.* (2014) was followed. Briefly, the DNA samples were amplified using the two universal eukaryote primers 18S-82F (5′-GAAACTGCGAATGGCTC-3′; López-Garcia *et al.* 2003) and Euk-516r (5′-ACCAGACTTGCCCTCC-3′; Amann *et al.* 1990), designed to amplify the variable V2 and V3 eukaryote 18S rRNA gene regions. Polymerase chain reactions described in Georges *et al.* (2014) were carried out with 10 ng of environmental DNA as a template. Tag-pyrosequencing was carried out by the company GenoScreen (Lille, France) in a 1/4 plate run on a 454 GS FLX Titanium sequencer. Pyrosequences were submitted to GenBank-SRA under the accession number SRP041236.

The pyrosequences were processed using the MOTHUR 1.28.0 software (Schloss *et al.* 2009) following the standard operating procedure (Schloss, Gevers and Westcott 2011). The dereplicated 'clean' sequences were aligned against the SILVA 108 database (http://www.arb-silva.de/). Around 7% of the sequences suspected of being chimeras were removed using the UCHIME software (Edgar, 2010). The remaining sequences were clustered into OTUs (operational taxonomical units) at a 97% similarity threshold. Singletons in one sample may not be single for the whole data set; for this reason, only unique amplicons that occurred exclusively in only one sample (single-singletons) were removed from downstream analyses, as these are most probably erroneous sequencing products (Reeder and Knight 2009). To enable comparison between samples, the data set was subsampled to the lowest number of sequences in one sample (1092 sequences). Finally, all OTUs were given a putative taxonomic affiliation based on BLAST (Altschul *et al.* 1990) identification of the closest relatives against the PR2 database (Guillou *et al.* 2013), and 8662 sequences affiliated to Alveolata were extracted from this data set for the purposes of this study.

Microscopic identification and enumeration

For dinoflagellate and ciliate enumeration, 500 mL samples were taken from the 0–300 m water column of each station (Table 1) at 6–11 depths (Supplementary Table S1). The samples were placed in opaque glass bottles, fixed with acid Lugol's solution (2% v/v) and stored at 4°C in the dark until analysis. In the laboratory, samples were left to settle for 3–4 days at 4°C. The bottom 100 mL of each sample was transferred into Hydrobios settling chambers, allowing them to settle for a minimum of 16 h, and then they were examined with an inverted microscope (Nikon Eclipse TE2000-S; ×400). Ciliates and dinoflagellates were identified based on their morphology (morphospecies) at the lowest possible taxonomic level (Tomas 1997; McMinn and Scot 2005; Petz 2005; Hoppenrath, Elbrächter and Drebes 2009). Ciliates and dinoflagellates were further divided into six size groups (<20, 20–40, 40–60, 60–80, 80–100 and >100 mm). Linear dimensions were measured at ×400 magnification using an image analyzer with a camera mounted on the microscope. Biovolumes of cells were calculated assuming the nearest geometrical shape; for this, a minimum of 10 cells (for rare morphospecies) and a maximum of 300 cells (for the most abundant morphospecies) were measured. Biovolumes were converted to carbon biomass based on a C:biovolume factor of 0.19 pg C μm^{-3} (Putt and Stoecker 1989) for ciliates and on the C:biovolume algorithm for heterotrophic dinoflagellates (Mender-Deuer and Lessard 2000).

Pigment measurements

The pigment analysis was performed as described in Lasbleiz *et al.* (2014). Briefly, 1–2.2 L of seawater were filtered through 25 mm Whatman GF/F filters. Extracts were analyzed by high-performance liquid chromatography (HPLC) with a complete Agilent Technologies 1200 series system. Thirteen pigments (see Supplementary Table S2) were used as signatures of major phytoplankton groups. Since different phytoplankton groups can share the same pigment, the pigment assignment was based on the most characteristic pigments for each group. The pigments were grouped into the following two major categories: (i) microphytoplankton—associated with Fucoxanthin and Diatoxanthin (diatoms), and Peridin and Diadinoxanthin (dinoflagellates); and (ii) pico- and nanoplankton—associated with the other nine pigments (see Supplementary Table S2). Note that diatoms dominated the microphytoplankton at all stations,

Downloaded from http://femsec.oxfordjournals.org/ by guest on October 6, 2016

representing between 30% (E-1) and 90% (F-L) of the total plankton carbon biomass at the fertilized stations (Lasbleiz *et al.* 2014).

Data analysis

In order to identify the most 'enhanced' ciliates and dinoflagellates in relation to the iron fertilization, the ratio of mean integrated abundance of cells in the ML was calculated based upon microscopy data. This was then compared spatially between the iron-fertilized stations and the HNLC R-2 station, and temporally at stations A3 and E. Morphospecies with a ratio >3 were considered as 'enhanced'. For tag-pyrosequencing data, only the most abundant OTUs with relative abundance >1% of the total Alveolata sequences were considered. OTUs with relative sequence abundance more than three times higher relative to a reference station were considered as 'enhanced'. By choosing such a stringent criterion, the risk was reduced of an 'enhanced' morphospecies/OTU being solely the consequence of the disappearance of another morphospecies/OTU (Landa *et al.* 2015). Morphospecies or OTUs not detected at the HNLC R-2 station, but observed at an iron-fertilized station, were considered as 'enhanced' by the iron fertilization.

The quantitative data of dinoflagellate and ciliate counts, and pigment concentrations from the different samples, were compared using the Plymouth routines in the multivariate ecological research (PRIMER v.6) software package (Clarke and Gorley 2006). For cluster analysis, only the samples of the ML were considered. The Bray–Curtis dissimilarity coefficients were analyzed by cluster analysis on square-root values. The similarity profile (SIMPROF) permutation test was conducted in PRIMER v.6 to establish the significance of dendrogram branches resulting from cluster analysis.

RESULTS

Study area

The result of the interaction between the Antarctic Circumpolar Current and the local bathymetry triggered a higher iron supply. This, in turn, caused the occurrence of several blooms within the study site (Fig. 1a and b). Any chlorophyll (Chl) *a* concentration in the surface mixed layer $\geq 0.6\ \mu g\ L^{-1}$ is considered a bloom situation (Lasbleiz *et al.* 2014), which is about twice the $\leq 0.3\ \mu g\ L^{-1}$ representative for the HNLC Southern Ocean. The HNLC reference station R-2 was characterized by low Chl *a* concentrations ($0.28\ \mu g\ L^{-1}$) in the ML (Table 1) and by a surface temperature of 2.1°C (Fig. 2). The stations situated in the iron-fertilized waters were characterized by higher Chl *a* concentrations (Fig. 2; Table 1). During early spring (October–November), station A3 had a deep ML (~150 m) and concentrations of Chl *a* increased by 3-fold between the first (A3-1) and the second visit 28 days later (A3-2, Fig. 2; Table 1). The three stations (E-1, E-3 and E-5) sampled temporally showed an increase in Chl *a* values between 0.6 and $1.2\ \mu g\ L^{-1}$ in the ML (40–70 m; Fig. 2; Table 1). The F-L station reached a Chl *a* concentration of $4\ \mu g\ L^{-1}$ and was constrained in a shallow ML (40 m). The highest temperature in the ML was at the F-L station, indicating the influence of sub-Antarctic waters (Fig. 2). The macronutrient concentrations in the ML at all stations were always high, and not limiting for phytoplankton growth (Table 1; see also Supplementary Fig. S1). The dissolved iron concentration (dFe) was variable (Quéroué *et al.* 2015), while noting that iron stocks do not necessarily reflect fluxes, since the iron can be consumed at the same rhythm as it arrives from the plateau (S. Blain, personal communication).

Morphological observations and tag-pyrosequencing results

Morphological observations allowed the identification of 97 morphospecies belonging to 60 dinoflagellates and 37 ciliates (Table 2; for a detailed list see Supplementary Table S3). Within the 37 ciliate morphospecies, 25 were aloricate and 12 loricate (tintinnids). The highest number of identified morphospecies of ciliates and dinoflagellates was observed at stations A3-1 and E-5 (30), while the lowest was recorded at station F-L (23). N/A: not available.

In addition, tag-pyrosequencing revealed 196 Alveolata-related OTUs belonging to 36 taxa (Table 2; for a detailed list see Supplementary Table S4). Dinoflagellates were the most

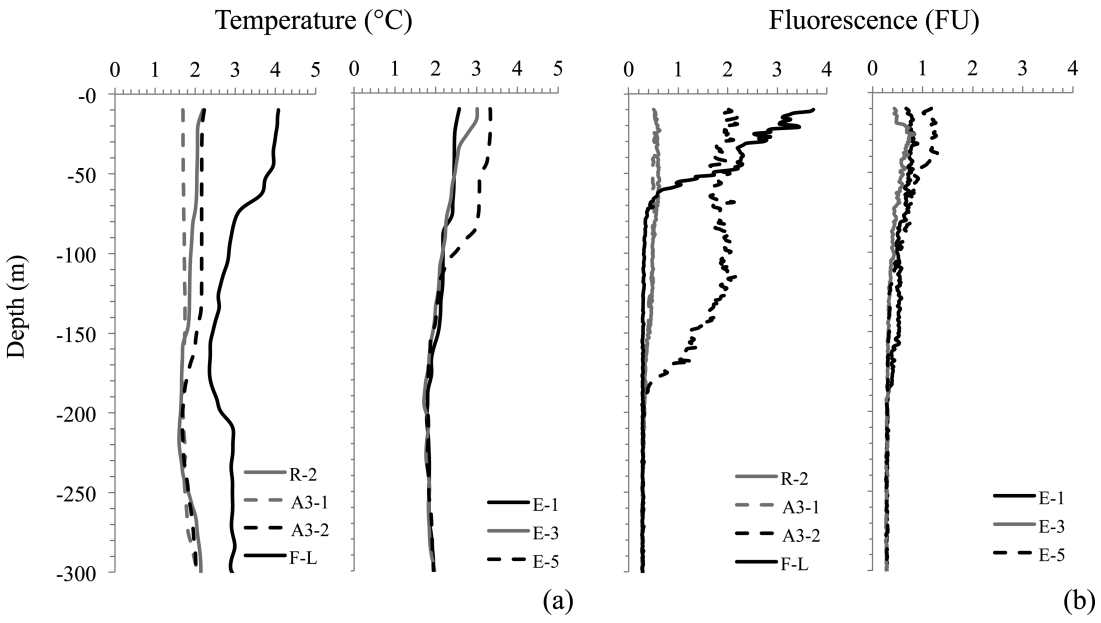

Figure 2. Profiles of temperature (**a**) and Chl *a* as derived from *in vivo* fluorescence (**b**) for each of the sampled stations.

Downloaded from http://femsec.oxfordjournals.org/ by guest on October 6, 2016

Table 2. Top: Number of genera and related 'morphospecies' (i.e species defined on their morphological characteristics) based on microscopy and number of higher taxonomic groups (taxa), OTUs and sequences, based on tag-pyrosequencing data. OTUs were defined at 97% sequence similarity. Bottom: number of dinoflagellate and ciliate morphospecies observed by microscopy and number of Alveolata-related OTUs obtained by tag-pyrosequencing in each station. N/A: not available.

		Microscopy		Tag-pyrosequencing		
		Genera	Morphospecies	Taxa	OTUs	Sequences
Dinoflagellates	16	60	22	73	5968	
Ciliates	Aloricate	13	25	8	20	415
	Loricate	12	12	2	3	30
	Total	25	37	10	23	445
MALVs	Group I			1	28	1509
	Group II			1	68	641
	Group III			1	8	93
	Group V			1	2	6
	Total			4	100	2249

	Microscopy	Tag-pyrosequencing	
Station	Morphospecies	OTUs	Sequences
R-2	28	82	1508
A3-1	30	N/A	N/A
A3-2	29	102	1093
F-L	23	78	1542
E-1	26	111	1194
E-2	26	129	1604
E-3	30	27	1727

abundant higher taxonomic group, representing 69% of the total number of sequences, followed by MALVs (26% of the total number of sequences), which, with 100 OTUs, were the most diverse (Table 2). Finally, 445 sequences (5% of the total alveolate sequences) belonging to 23 OTUs were affiliated to ciliates, with 20 OTUs affiliated to aloricates and three to loricates. Apicomplexa were represented by only two OTUs (data not shown).

Temporal and spatial community distribution

Microscopy

Dinoflagellates were about one order of magnitude more abundant than ciliates (Fig. 3a–d). The HNLC reference station R-2, and station A3-1, showed low dinoflagellate abundances and few variations with depth (Fig. 3a). At the A3-2 and F-L fertilized stations, the maximum abundances were recorded near the

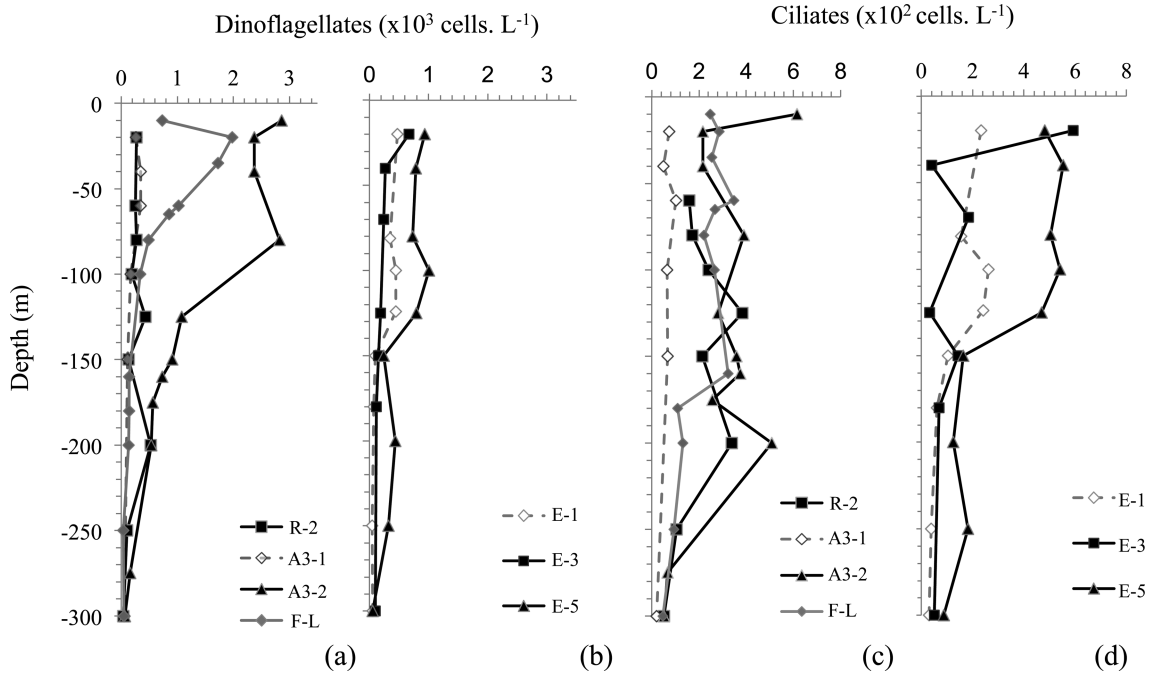

Figure 3. Vertical profiles of dinoflagellate (**a**, **b**) and ciliate (**c**, **d**) abundances.

Downloaded from http://femsec.oxfordjournals.org/ by guest on October 6, 2016

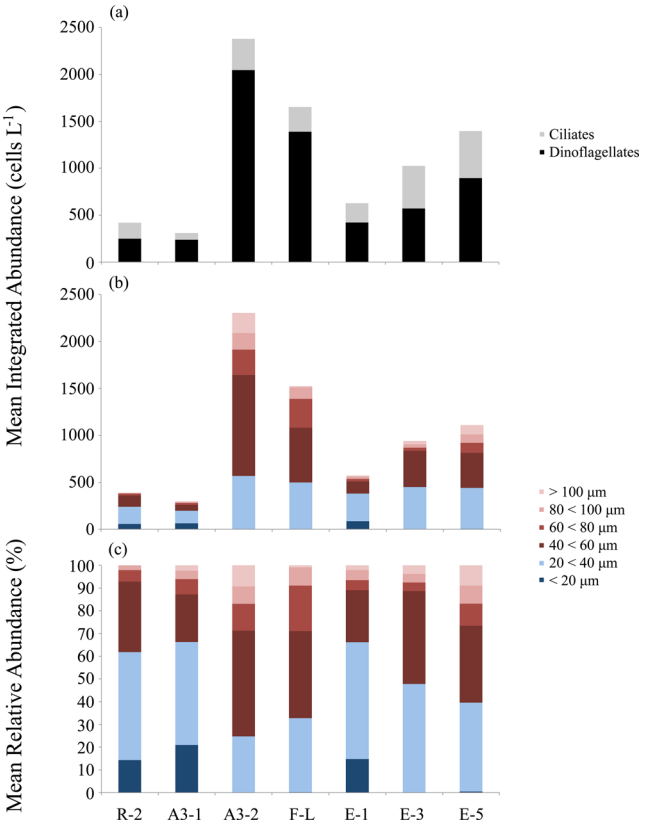

Figure 4. Mean integrated abundance of cells (**a**), size classes (**b**) and the relative abundance of size classes (**c**) of ciliates and dinoflagellates in the ML (mixed layer cf. Table 2) of each station.

base of the ML. The temporal distribution of the mean integrated abundance of dinoflagellates showed an 8.5-fold increase in the ML of the A3 stations (from 238 cells L^{-1} at A3-1 to 2046 cells L^{-1} at A3-2; Fig. 4a; Supplementary Table S3). The temporally sampled E stations showed a modest increase of ~2-fold (from 422 cells L^{-1} at E-1 to 896 cells L^{-1} at E-5; Fig. 4a; Supplementary Table S3), and their maximum abundances were recorded at E-5, just below the ML (Fig. 3b). The most abundant genera in the dinoflagellate community were *Gymnodinium* spp., *Gyrodinium* spp., *Protoperidinium* spp. and *Amphidinium* spp. (Supplementary Table S3), which accounted for 93 ± 3% (mean ± SD) of the total number of dinoflagellates at all stations.

Ciliate mean integrated abundances in the ML ranged from 75 ± 19 cells L^{-1} at A3-1 to 510 ± 37 cells L^{-1} at E-5. A clear increase in the mean cell abundance was observed between stations A3-1 and A3-2 (5-fold), and E1 and E5 (2-fold), sampled temporally (Figs 3c and d, and 4a). Overall, at the HNLC R-2, A3-1 and E-1 stations, <40 μm cells represented an important part (>60%) of the dinoflagellate and ciliate community (Fig. 4b and c). In contrast, >40 μm cells increased in abundance at the A3-2, F-L, E-3, and E-5 stations (Fig. 4b and c). Within ciliates, aloricates dominated in number of cells in the ML. At the HNLC R-2 station and A3-1, <20 μm cells belonging to *Strobilidium* sp., *Myrionecta* sp. and *Lohmaniella* spp. represented an important part of the aloricate community (Supplementary Table S3). In addition, >20 μm cells belonging to *Strombilidium* spp. and *Laboea* spp. represented an important part of the aloricates at A3-2, F-L and the 'E' stations (Supplemetnary Table S3). Within loricates, small sized *Codonellopsis* spp. dominated at the R-2 station, while the medium to large-sized (40–120 μm) *Cymatocylis* spp. showed a high relative abundance at the A3-1 and A3-2 stations. An important proportion (50%) of *Acanthostomella norvegica* was observed at station F-L and the E stations (Supplementary Table S3).

Tag-pyrosequencing

According to tag-pyrosequencing, OTUs related to *Gyrodinium* spp., *Gymnodinium* spp. and *Warnowia* spp. were the most abundant sequences in all samples (Fig. 5). *Gyrodinium* spp. accounted for 36% of the dinoflagellate sequences at stations R-2 and F-L; and 85, 20 and 98% at stations A3-2, E-1 and E-5, respectively (Fig. 5). *Strombidiidae*-affiliated sequences dominated the ciliate-related sequences in all samples (65 ± 8%, mean ± SD), except in the E-5 sample (Fig. 5), where only two ciliate-related sequences were detected. (Supplementary Table S3). A much higher proportion of *Strobilididae* was observed at the HNLC R-2 station compared with the fertilized stations (Fig. 5). In addition to microscopy observations, tag-pyrosequencing revealed MALV-related sequences. In this group, MALV I and MALV II dominated in every sample (Fig. 5).

Response to the natural iron fertilization

Microscopy data and pyrosequencing were in accordance in capturing frequency shifts of some of the most abundant taxa. For example, dinoflagellates belonging to *Gyrodinium* were found to be 'enhanced' in both data sets. In comparison with station R-2, *Gyrodinium* spp. were found to be 'enhanced' at stations A3-2, FL (Table 3) and E5 (Table 4). In addition, *Gymnodinium* spp. were found to be highly 'enhanced' at station A3-2, while the most 'enhanced' genus at station F-L was *Protoperidinium* spp. (Table 3). For stations sampled temporally, all the dinoflagellates were found to be 'enhanced' between stations A3-1 and A3-2 (Table 3), while only 2–3 were 'enhanced' between stations E-1 and E-5 (Tables 3 and 4). Concerning ciliates, the abundant Strombiidae spp. were identified as 'enhanced' at F-L (Table 3) and at all fertilized stations, except E-5 (Table 4). It is noteworthy that, from the microscopy data, the tintinnid *Cymatocylis calicyformis* was considered as 'enhanced' at all iron-fertilized stations except F-L, while *Cymatocylis* spp. and *Salpingella* sp. were identified as 'enhanced' between stations A3-1 and A3-2 (Table 3). MALVs were only identified through pyrosequencing. In pyrosequencing data, MALV OTUs represented the most sensitive group to iron enrichment, with 14 OTUs considered as 'enhanced' by the natural fertilization (Table 4). Among these 14 OTUs, four were detected only at the iron-fertilized stations.

Similarities between stations

Microscopy

Group-average cluster analysis based on Bray–Curtis dissimilarity of the dinoflagellate and ciliate abundance data in the ML indicated four clusters at 60% similarity composed of: (i) the R-2 samples; (ii) the E-1, E-3 and E-5 samples; (iii) the A3-2 and F-L samples; and (iv) the A3-1 samples (Fig. 6a). The four clusters were significantly different from each other (ANOSIM test, $R = 0.81$, $P < 0.001$). At a higher level of similarity (between 65% and 90%), the samples clustered according to their respective station (Fig. 6a).

Pigments

The concentration of group pigment signatures to Chl *a* ratios showed that pico- and nanoplankton groups, and in particular Prymnesiophyceae, prevailed at the HNLC reference R-2 station

Downloaded from http://femsec.oxfordjournals.org/ by guest on October 6, 2016

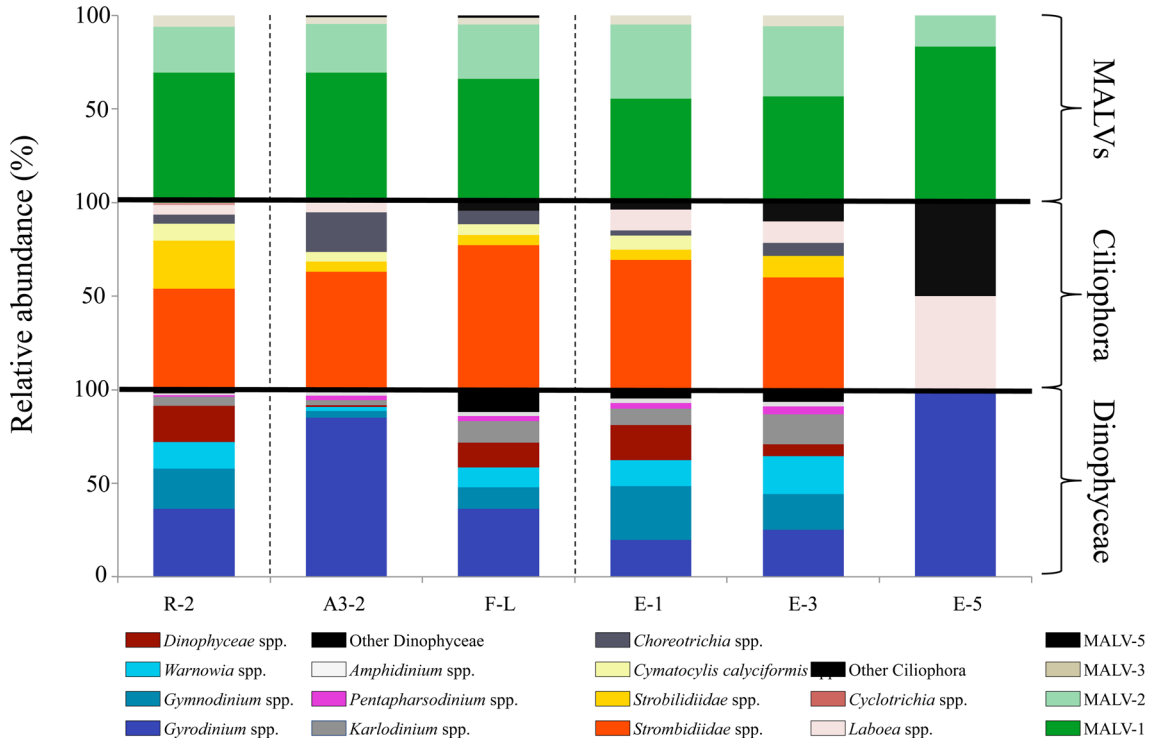

Figure 5. Relative abundance of higher taxonomic groups represented by >1% of the total number of sequences.

(Table 5). A higher ratio of Fucoxanthin + Diatoxanthin to Chl *a*, illustrating a diatom dominance, was observed at the A3-2 (44.1 ± 4.5%) and F-L stations (48.3 ± 3.6%, Table 5). The 4-fold decrease in pico- and nanoplankton pigments, and a slight increase (~6%) in Fucoxanthin and Diatoxanthin ratios to Chl *a* that occurred between stations A3-1 and A3-2 (Table 5), also illustrates the replacement of smaller cells (pico- and nanoplankton) by larger smaller ones (diatoms) during development of the bloom. Similar, but less pronounced trends were also observed between stations E-1 and E-5 (Table 5). Group-average cluster analysis based on the Bray–Curtis dissimilarity of pigment concentrations in the ML (Fig. 6b) indicated four clusters at 73% similarity: (i) the HNLC R-2 samples; (ii) the E and A3-1 samples; (iii) the A3-2 samples; and (iv) the F-L samples. The four clusters were significantly different from each other (ANOSIM, $R = 0.97$, $P = 0.001$).

Relationships between dinoflagellates, ciliates and pigment signatures

Dinoflagellates were significantly related to Chl *a*, and diatom and pico-nanoplankton pigments, while no relationship was found between ciliates and any phytoplankton pigments. Considering several of the most abundant genera of dinoflagellates such as *Gyrodinium*, *Gymnodinium*, *Amphidinium* and *Protoperidinium*, the relationships with fucoxanthin and diatoxanthin associated with diatoms were always either significant ($P < 0.05$) or highly significant ($P < 0.001$), while only *Amphidinium* showed some relationship with pico-nanoplancton pigments (Table 6). In contrast, the most abundant ciliates (e.g *Strombidium* spp. and *Cymatocylis calyciformis*) did not show any significant relationship with Chl *a* or any other pigments. Finally, the 60–80 μm size class of microzooplankton showed the highest relationship with Chl *a* ($P < 0.0001$).

DISCUSSION

Community structure and response to phytoplankton blooms

According to KEOPS2's microscopical observations and pigment analysis data, diatoms dominated the phytoplankton community in all of the blooms, while nano- and picophytoplankton, and in particular Prymnesiophyceae, characterized the HNLC R-2 station (Georges *et al.* 2014; Lasbleiz *et al.* 2014; Sackett *et al.* 2014; Table 5). The cluster analysis of samples based on dinoflagellate and ciliate abundance data and phytoplankton pigments showed a distinction between the fertilized stations (A3, 'E' and F-L) and the HNLC R station. Since the bloom starts in early November, reaches its maximum level in late November–early December and collapses in January–February (Mongin, Molina and Trull 2008; Blain *et al.* 2013), stations A3-1 and E-1 were sampled very early in the season and could be characterized as 'false reference sites' (Landa *et al.* 2015). In addition, the 'E' stations (E-1, E-3 and E-5) were situated within a complex meander south of the polar front that was relatively isolated, and the peak of the phytoplankton bloom, according to satellite images, occurred several weeks after the end of the study cruise.

The maximum abundances of dinoflagellates and ciliates were often observed at the base of the ML (Table 1, Fig. 3) and coincided with the formation of the deep chlorophyll maximum (DCM) (Lasbleiz *et al.* 2014). The formation of a DCM is described as a recurrent feature in the Southern Ocean, and is explained by the accumulation of inactive, though living, algal cells, mainly composed of diatoms (Uitz *et al.* 2009 and references therein). Mobile protists, such as nanoflagellates, dinoflagellates and ciliates, have the ability to feed on particle-associated prey and then detach (Kiørboe *et al.* 2003). Suspended or sessile protist feeders can also use sinking organic matter aggregates (Artolozaga *et al.* 1997; Christensen-Dalsgaard and Fenchel 2003).

Downloaded from http://femsec.oxfordjournals.org/ by guest on October 6, 2016

Table 3. Heatmap of the morphospecies identified by microscopy as 'enhanced' (i.e with >3 cell abundance increase in the mixed layer) in at least one of the stations used for the comparisons with R-2 or for temporal comparisons between A3-2/A3-1 and E-5/E-1.

Groups	R-2	Relative to the HNLC R-2 station							Temporal between		Temporal between
		A3-1	A3-2	F-L	E-1	E-3	E-5		A3-2/A3-1		E-5/E-1
Dinoflagellates											
Amphidinium spp.		--			--	--	--				--
Ceratium. pentagonum		--									
Gonyaulax sp.											--
Gymnodinium spp.		--									--
Gyrodinium spp.		--			--	--	--				
Protoperidinium depressum		--									--
Protoperidinium spp.		--									--
Scripsiella sp.											
Ciliates (Aloricate)											
Laboea strobila		--	--	--		--					--
Leegardiella spp.		--					--		--		--
Lohmaniella sp.		--		--	--		--				--
Myrionecta spp.				--		--	--		--		--
Rimostrombidium sp.		--									--
Strobilidium spp.		--			--		--				--
Strombidium acutum				--							
Strombidium spp.		--		--	--						--
Strombidium sulcatum		--							--		
Tontonia spp.		--					--				--
Ciliates (Loricate)											
Acanthostomella norvegica			--								
Amphorides laackmanni		--					--				
Codonellopsis pusilla											
Codonellopsis soyai			--	--	--	--	--				
Cymatocylis antarctica											
Cymatocylis calyciformis									--		
Cymatocylis kerguelensis				--	--	--					
Cymatocylis parva				--	--	--	--				--
Salpingella sp.											--

Relative abundance of morphospecies:

Detected in the station with the one that the comparison is made (reference station, i.e R-2, A3-1 or E-1)	Not detected
%<1%	%<1%
1% <%< 10%	1% <%< 10%
10% <%< 20%	10% <%< 20%
20% <%< 30%	20% <%< 30%
30% <%< 40%	30% <%< 40%
% > 40%	%> 40%

Dashes (–) represent the morphospecies that were detected in the samples but were not considered as 'enhanced' since the cell abundance ratio with the reference station was <3 (see also the Material and methods and Supplementary Table S3). Note that morphospecies not detected at the HNLC R-2 station, but observed at iron-fertilized station, were considered as 'enhanced'. All stations were compared with the HNLC R-2 station; temporal comparisons between A3-2 relative to A3-1 and E-5 relative to E-1 were also made. The different shades represent the mean relative abundance in the ML. Blanks indicate absence of detection.

The response of herbivorous protists to iron fertilization is clearly indirect and is related to the increase of their phytoplankton prey (see also Supplementary Fig. S1). Information about microzooplankton in iron enrichment experiments in the Southern Ocean is scarce, in particular for dinoflagellates (Table 7). Interestingly, while ciliates and dinoflagellates have similar growth rates, dinoflagellates form denser populations in terms of cell abundance and biomass under phytoplankton bloom conditions (Sherr and Sherr 2007 and references therein; Table 7). A possible advantage that dinoflagellates may have over ciliates may well be that they are effective predators of diverse taxa (from bacteria to metazoa) due to their varied feeding mechanisms (reviewed in Sherr and Sherr 2009; Jeong *et al.* 2010); as a result, heterotrophic dinoflagellates have a broader prey selection and, in this study, were most probably consuming ciliates too. Consequently, while the dinoflagellates were significantly related to their potential prey, the low ciliate abundances and the absence of any significant relationship with their potential nano- and picophytoplankton prey (Table 6) can be attributed to stronger top-down control by both dinoflagellates and metazoa.

Among all herbivorous protists, dinoflagellates have the greatest potential to consume large chain-forming diatoms (Sherr and Sherr 2007 and references therein). Diatom-consuming dinoflagellates, such as the athecate *Gyrodinium* spp. (Hansen 1992; Neuer and Cowles 1994; Strom and Strom 1996; Putland 2000; Horner *et al.* 2005; Saito *et al.* 2005; Grattepanche *et al.* 2011a) and the thecate *Protoperidinium* spp. (Jacobson and Anderson 1993; Buskey 1997; Sherr and Sherr 2007), were found

Downloaded from http://femsec.oxfordjournals.org/ by guest on October 6, 2016

Table 4. Heatmap of the OTUs detected by tag-pyrosequencing as 'enhanced' (i.e with >3 sequence abundance increase in the mixed layer) in at least one of the stations used for the comparisons with R-2 or for temporal comparisons between A3-2/A3-1 and E-5/E-1.

OTU affiliation	R-2	Relative to the HNLC R-2 station						E-5/E-1
		A3-2	F-L	E-1	E-3	E-5		
Dinoflagellates								
Dinoflagellates sp.		--	--		--			
Gyrodinium rubrum			--		--			
Gyrodinium spirale		--	--	--	--			
Karlodinium micrum			--			--		--
P. tyrrhenicum.			--					
Warnowia sp.		--	--	--		--		--
Ciliates								
Scuticociliatia spp.								
Laboea strobila			--	--	--			
Strombidiidae spp.								
MALVs								
Group I clade 1		--		--	--	--		--
Group I clade 1			--					
Group I clade 1			--			--		--
Group I clade 4				--	--	--		--
Group I clade 4			--		--			
Group I clade 5								
Group II sp.								
Group II clade 10 and 11								
Group II clade 10 and 11			--		--	--		--
Group II clade 13								
Group II clade 16		--	--		--			
Group II clade 5		--		--	--	--		
Group II clade 6								
Group III		--		--	--			

Relative abundance of OTUs:

Detected in the station with the one that the comparison is made (R-2, or E-1)	Not detected in the station with the one that the comparison is made (R-2, or E-1)
%<1%	%<1%
1% <%< 10%	1% <%< 10%
10% <%< 20%	10% <%< 20%
20% <%< 30%	20% <%< 30%
30% <%< 40%	30% <%< 40%
% > 40%	%> 40%

Dashes (–) represent the morphospecies that were detected in the samples but were not considered as 'enhanced' since the cell abundance ratio with the reference station was <3 (for more details see also the Material and methods and Supplementary Table S3). Note that OTUs not detected at the HNLC R-2 station, but observed at an iron-fertilized station, were considered as 'enhanced'. All stations were compared with the HNLC R-2 station; temporal comparisons between E-5 relative to E-1 were also made. The different shades represent the mean relative abundance in the ML. Blanks indicate absence of detection. Note that A3-1 was not sampled for molecular analysis.

Downloaded from http://femsec.oxfordjournals.org/ by guest on October 6, 2016

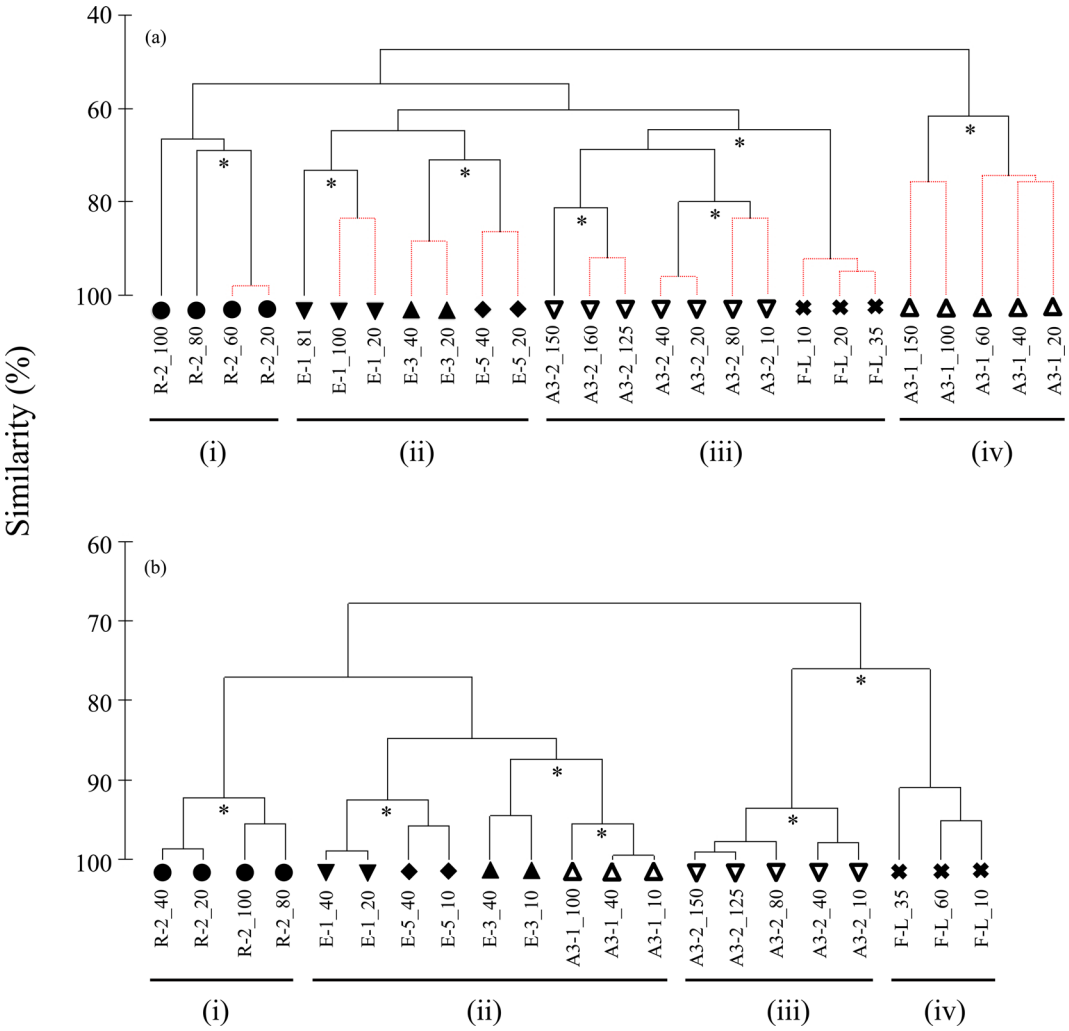

Figure 6. Group-average cluster analysis based on the Bray–Curtis similarity matrix of square-root-transformed ciliate and dinoflagellate cell abundances (**a**) and pigment concentrations (**b**). Asterisks at nodes in the dendrogram indicate significant differences between bifurcations ($P < 0.05$). (b). Phytoplankton group-specific marker pigments are listed in Supplementary Table S2.

to be among the most enhanced dinoflagellate taxa in both microscopy and pyrosequencing data, and showed significant relationships with phytoplankton (Tables 3, 4 and 6). A strong response was also observed for the Gymnodinoid dinoflagellates (Table 3) such as *Gymnodinium* spp., which, depending on their size, feed on a broad prey spectrum, from coccoid cyanobacteria (Strom 1991) to small eukaryotic phytoplankton (Sherr, Sherr and McDaniel 1991) to large diatoms (Hansen, 1992).

Based on trophic organization, HNLC areas seem conceptually similar to oligotrophic regions dominated by small producers and consumers (e.g. Hall and Safi 2001; Oliver *et al.* 2004; Obernosterer *et al.* 2008; Christaki *et al.* 2008, 2014). It was noteworthy that <20 μm aloricate ciliates were related to the HNLC R-2 and A3-1 stations, while >20 μm cells belonging to *Strombilidium* spp. and *Laboea* spp. represented an important part of the aloricates at A3-2, F-L and the 'E' stations, (Fig. 4; Supplementary Table S3). Similarly, the small-sized *Codonellopsis* spp. was dominant at the R-2 station, while the medium to large-sized (40–120 μm) *Cymatocylis* spp. showed a high relative abundance at the A3 stations. High abundances of *Cymatocylis* spp. were also observed at the A3 stations at late stages of the phytoplankton bloom (Christaki *et al.* 2008).

MALV OTUs represented a sensitive group to iron enrichment, with 14 OTUs considered as 'enhanced' by the natural fertilization (Table 5). The considerable abundance and diversity of MALVs suggest interactions with various hosts, and therefore it has been proposed that the whole MALV assemblage is composed of marine parasites (Skovgaard *et al.* 2005; Massana and Pedrós-Alió 2008). Most of the sequences belonged to MALV I, which have a wide host spectrum, whereas MALV II are considered as dinoflagellate parasites (Massana *et al.* 2011), so their enhanced presence at the iron-fertilized stations can be explained by their association with dinoflagellate cells.

In the rare studies combining morphological and molecular results, it has been made clear that they cannot be directly compared (Savin *et al.* 2004; Doherty *et al.* 2007; Monchy *et al.* 2012). In this study, morphological analyses and pyrosequencing were generally in accordance with capturing frequency shifts of abundant taxa. Tag-pyrosequencing gave a broad alveolate community picture, including ciliates, dinoflagellates and MALVs. However, certain inconsistencies between the two methodologies were observed. For example, 12 morphospecies of tintinnids were observed with microscopy while only three OTUs were retrieved from pyrosequencing (Supplementary Tables S2 and S3).

Downloaded from http://femsec.oxfordjournals.org/ by guest on October 6, 2016

Table 5. Ratios (in %) of phytoplankton group pigment signatures to Chl *a* concentrations in the mixed layer of each station (mean ± SD).

	Fuco + Diato:Chl *a*	19′-Hexano:Chl *a*	Pico-nano:Chl *a*
R-2	27.1 ± 1.7	22.3 ± 3.7	51.8 ± 1.8
A3-1	38.5 ± 2	6.8 ± 0.8	21.3 ± 3.8
A3-2	44.1 ± 4.5	1.4 ± 0.2	5.1 ± 0.7
F-L	48.3 ± 3.6	1.6 ± 0.6	4 ± 1.3
E-1	44.1 ± 6.3	8.9 ± 2.2	23 ± 6
E-3	37.2 ± 6.5	11.8 ± 4.5	22.4 ± 13.3
E-5	49.2 ± 0.4	9 ± 1.9	16.3 ± 7.7

Fucoxanthin + Diatoxanthin and 19′-Hexanoyloxyfucoxanthin were considered as major diatom and Prymnesiophyceae characteristic pigments, respectively. The percentage of pico- and nanoplankton sized phytoplankton corresponds to the sum of the pigments of Chlorophyceae, Pelagophyceae, Prymnesiophyceae and Prasinophyceae to Chl *a* (listed in detail in Supplementary Table S2).

Table 6. Determination coefficients (r^2) of the statistically significant log–log linear regressions of the abundances of dinoflagellates, *Gyrodinium* spp., *Gymnodinium* spp., *Amphidinium* spp. and *Protoperidinium* spp., different dinoflagellate + ciliate size classes versus Chl *a* and major pigment signatures of phytoplankton.

Parameter 1: cells L^{-1}	Parameter 2: pigment concentration $\mu g\ L^{-1}$	*n*	r^2
Dinoflagellates	Chl *a*	37	0.31**
Dinoflagellates	Diatoms	37	0.21*
Dinoflagellates	Pico-nanoplankton	37	0.25*
Gyrodinium spp.	Diatoms	37	0.27**
Gyrodinium spp.	Pico-nanoplankton	37	0.12*
Gymnodinium spp.	Diatoms	37	0.42***
Amphidinium spp.	Diatoms	37	0.21*
Amphidinium spp.	Pico-nanoplankton	37	0.14*
Protoperidinium spp.	Diatoms	37	0.48***
20 – 40 μm size class	Chl *a*	36	0.21*
40 – 60 μm size class	Chl *a*	36	0.15*
60 – 80 μm size class	Chl *a*	36	0.40***
80 – 100 μm size class	Chl *a*	36	0.28**

Diatoms were considered to be associated with fucoxanthin + diatoxanthin. Pico + nanoplankton pigments used here are listed in Suppementary Table S2. The ciliates did not show any significant relationship.
*$P < 0.05$, **$P < 0.001$, ***$P < 0.0001$.

This may be due to: the recurrent problems of BLAST-derived taxonomy, especially at low-level taxa, which are related to the sequence length; the universality of the primers; the variability of the 18S region; and/or the database coverage for the specific taxonomic group (e.g. Bik *et al.* 2012). In addition, the choices in the sequence treatments may also strongly affect the discrepancy between molecular and morphological analyses as described in Bachy *et al.* (2013).

Potential role of ciliates and dinoflagellates as phytoplankton consumers, and as prey of mesozooplankton in blooms

Stocks, rates and export, determined during the KEOPS1 and 2 projects, suggested a 'budget' for the flow of carbon through microbial and higher trophic levels (Christaki *et al.* 2014). It was shown that large differences could be observed between the early phase (KEOPS2) and the late phase (KEOPS1) of the bloom. During KEOPS1 in summer 2005, microzooplankton grazing was the main factor regulating phytoplankton biomass in the bloom

Table 7. Comparison of ciliates, dinoflagellates and zooplankton abundance and biomass, following natural and artificial iron fertilization in the Southern ocean.

		Ciliates				Dinoflagellates				Mesozooplankton			
		(10^3 cells m^{-3})		(mg C m^{-3})		(10^3 cells m^{-3})		(mg C m^{-3})		(mg C m^{-3})			
		Out	In	Out	In	Out	In	Out	In	Out	In		
Southern Ocean													
Natural	KEOPS2	113	333	0.42	1.24	167	2127	0.92	7.46	2	4	This study	
												Carlotti *et al.* (2015)	
	KEOPS1	107	197	0.43	1.70	–	–	–	–	36	72	Christaki *et al.* (2008)	
												Carlotti *et al.* (2008)	
								3.24	46.8	–	–	Poulton *et al.* (2007)	
	CROZEX	–	–	0.48	2.76								
Artificial	EisenEx	13	61	0.05	0.2	65	113	1.28	0.34	7.2	14.4	Henjes *et al.* (2007)	
	SOIREE	465	1342	0.74	1.7	–	–	–	–	22.8	30.1	Hall and Safi (2001); Zeldis (2001)	

Out, values reported for HNLC waters; in, values reported for iron-fertilized patches. –: not done. For KEOPS2 (early bloom) and KEOPS1 (late bloom), the integrated values are for the ML. KEOPS1, KEOPS2: mean integrated abundance and biomass in the ML, 'in' are the maximum values recorded at A3 station (Fig. 1). CROZEX: surface values from Poulton *et al.* table 1 (stations M6.2 and M3.4). EisenEx: mean integrated values from the upper 150 m. Ciliates refer only to tintinnids and dinoflagellates only to thecate >50 μm. SOIREE: values from the mixed layer (~60–65 m).

Downloaded from http://femsec.oxfordjournals.org/ by guest on October 6, 2016

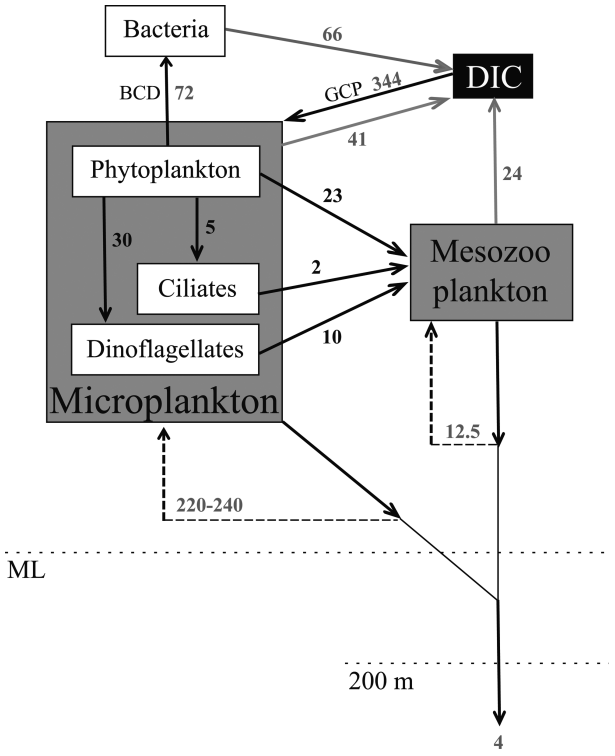

Figure 7. Schematic presentation of the carbon flow in the early stage of the bloom (KEOPS2) at the south-east bloom above the Kerguelen plateau (station A3-2). All fluxes are integrated over the ML, and units are in mmol C m^{-2} day^{-1}. Gray arrows indicate rates of respiration. Black arrows indicate the transfer of carbon between compartments and export. Dashed black arrows, going back to 'phytoplankton' and 'mesozooplankton', indicate possible accumulation of their biomass per day, once the respiration and export were subtracted. The values in gray, relative to phytoplankton, bacteria, mesozooplankton and export are detailed in Christaki *et al.* (2014) and are presented here to accompany the picture around the phytoplankton–microzooplankton–mesozooplankton carbon flow. Briefly: gross community production (GCP) measured from O_2 fluxes and converted into C fluxes using PQ = 1.8 (Cavagna *et al.* 2014). BCD: bacterial carbon demand (BCD = bacterial production + bacterial respiration; Christaki et al. 2014). Mesozooplankton ingestion and respiration rates (Carlotti *et al.* 2015), POC-based accumulation of phytoplankton biomass (Lasbleiz *et al.* 2014), export fluxes at 200 m (Planchon *et al.* 2014). DIC, dissolved inorganic carbon; ML, depth of the mixed layer.

(Brussaard *et al.* 2008; Christaki *et al.* 2008). During KEOPS2, iron fertilization stimulated primary production, with integrated net primary production ~26-fold higher in the fertilized areas compared with the HNLC R-2 station (Cavagna *et al.* 2014). However, comparison of the POC (particulate organic carbon) flux at 200 m indicated that a minor fraction of this GCP (gross community production) was exported during the early stage of the bloom, and a major one during the late phase (1.2% versus 26.3%; Christaki *et al.* 2014). The explanation of this surprising result was that during the early bloom period (KEOPS2), once respiration losses were subtracted from the GCP, ~200 mm C m^{-2} day^{-1} remained available in the water column for phytoplankton biomass accumulation and/or export. Measurements of POC accumulation in the water column over 5–10 days provided a very close estimate for phytoplankton biomass accumulation of 220–440 mm C m^{-2} day^{-1} (Fig. 7; Christaki *et al.* 2014; Lasbleiz *et al.* 2014). Another notable point is that while the absolute bacterial carbon channelled towards the higher trophic levels was quantitatively the same in spring and summer, the underlying mechanisms were contrasting. In spring, the BP (bacterial production) was relatively low, with most of it being channelled to the higher trophic levels due to predation. In summer, on the other hand, the BP was higher, but most of it had been returned to the dissolved phase through viral lysis (Christaki *et al.* 2014; Malits *et al.* 2014). The next step to this exercise was to add into the budget the potential role of microzooplankton as phytoplankton consumers and as prey for mesozooplankton. This was assessed from estimations of their production and carbon demand. Herbivorous protist growth rates are tightly related to prey concentration, with a threshold Chl *a* concentration for growth of between 0.1 and 2 μg Chl *a* L^{-1} and maximum growth between 0.25 and 5 μg Chl *a* L^{-1} (reviewed by Sherr and Sherr 2009). Since the growth rate of herbivorous protists is related to prey abundance, herbivorous protists would grow slowly at the onset of a bloom (Sherr and Sherr 2009). The POC doubling times of ~2 days were measured at stations F-L and A3-2, with the highest primary production growth rates of 0.3 day^{-1} (Cavagna *et al.* 2014). Considering all the above, ciliate and dinoflagellate production was estimated assuming a conservative growth rate $\mu = 0.23$ day^{-1}, which roughly corresponds to a generation time (GT) of 3 days [$\mu = \ln(2)/GT$]. This growth rate is also a compromise between the highest and lowest reported levels from incubation and dilution studies of natural communities between 0.2 and 1.4 day^{-1} (e.g. Bjørnsen and Kuparinen 1991; Verity *et al.* 1993; Neuer and Cowles 1994; Karayanni *et al.* 2008). Dinoflagellate and ciliate carbon demands were calculated assuming a growth efficiency (GE) of 30% (Straile 1997; Strom and Fredrickson 2008).

Ciliate and dinoflagellate carbon fluxes presented here (Fig. 7) are based on the assumptions that: (i) dinoflagellates and ciliates covered their carbon demand exclusively from phytoplankton; and (ii) all their potential production was grazed by mesozooplankton. Although these are fairly accurate estimations, the overall picture is balanced and consistent with several well-established facts: (i) dinoflagellates are potentially as important as consumers of phytoplankton as copepods are (e.g. Landry *et al.* 2000; reviewed in Sherr and Sherr 2007); (ii) herbivorous protists can cover an important percentage of the mesozooplankton carbon demand (e.g. Stoecker and Capuzzo 1990; Calbet and Saiz 2005; reviewed in Sherr and Sherr 2007); and (iii) although protists, and in particular dinoflagellates, have great potential in consuming phytoplankton, top-down control on microzooplankton partly explains the phytoplankton accumulation during the onset of the bloom (Strom 2002; reviewed in Sherr and Sherr 2009).

In conclusion, the microscopy and tag-pyrosequencing approaches in this study have provided an overview of the Alveolata assemblage in the HNLC waters and in the naturally fertilized blooms in the Southern Ocean. Similarity analysis has shown clear differences in the phytoplankton and microzooplankton community structures between the iron-fertilized and HNLC waters, and between the blooms, concerning their location and the fertilization mechanisms. Finally, carbon flux estimation through microzooplankton has suggested that the amount of phytoplankton biomass consumed by heterotrophic dinoflagellates in the ML during the onset of the Kerguelen bloom could be at least as great, if not greater, than that consumed by mesozooplankton.

Overall, as diatom blooms are responsible for a large part of carbon export in the sea following bloom senescence in general (e.g. Smetacek 1985; Sarthou *et al.* 2005) and in the Kerguelen region (e.g. Savoye *et al.* 2008), it is important to better represent some of the crucial but understudied links of carbon pathways that link phytoplankton, microzooplankton and mesozooplankton. In addition, consumption of diatoms by dinoflagellates also

Downloaded from http://femsec.oxfordjournals.org/ by guest on October 6, 2016

has implications for biogeochemical cycles through rejection of empty silica and/or production of mini-fecal pellets composed of more silica than carbon (e.g. Saito *et al.* 2005 and references therein).

SUPPLEMENTARY DATA

Supplementary data are available at FEMSEC online.

ACKNOWLEDGEMENTS

KEOPS was financed by INSU-CNRS, IPEV, ANR, and the French Ministry of Higher Education through a PhD grant. We thank our many colleagues who participated in the collection of various data sets, the KEOPS co-ordinator S. Blain, the chief scientist on board B. Quéguiner, and the crew aboard the R/V *Marion Dufresne* for their help in the successful completion of the cruise. www.englisheditor.webs.com is also thanked for the paper's English proofing. The color products for the Kerguelen area were produced by Ssalto/Duacs and CLS with support from Cnes. We thank two anonymous reviewers for their suggestions that improved the original manuscript.

Conflict of interest. None declared.

REFERENCES

Altschul SF, Gish W, Miller W, *et al.* Basic local alignment search tool. *J Mol Biol* 1990;**215**:403–10.

Amann RI, Binder BJ, Olson RJ, *et al.* Combination of 16S rRNA-targeted oligonucleotide probes with flow cytometry for analyzing mixed microbial populations. *Appl Environ Microbiol* 1990;**56**:1919–25.

Artolozaga I, Santamaria E, López A, *et al.* Succession of bacterivorous protists on laboratory-made marine snow. *J Plankton Res* 1997;**19**:1429–40.

Bachy C, Dolan JR, López-García P, *et al.* Accuracy of protist diversity assessments: morphology compared to cloning and direct pyrosequencing of 18S rRNA genes and ITS regions using the conspicuous tintinnid ciliates as a case study. *ISME J* 2013;**7**:244–55.

Bjørnsen PK, Kuparinen J. Growth and herbivory by heterotrophic dinoflagellates in the Southern Ocean, studied by microcosm experiments. *Mar Biol* 1991;**109**: 397–405.

Bik HM, Porazinska DL, Creer S, *et al.* Sequencing our way towards understanding global eukaryotic biodiversity. *Trends Ecol Evol* 2012;**27**:233–43.

Blain S, Capparos J, Guéneuguès A, *et al.* Distributions and stoichiometry of dissolved nitrogen and phosphorus in the iron-fertilized region near Kerguelen (Southern Ocean). *Biogeosciences* 2015;**12**:623–35

Blain S, Quéguiner B, Armand L, *et al.* Effect of natural iron fertilization on carbon sequestration in the southern ocean. *Nature* 2007;**446**:1070–4.

Blain S, Quéguiner B, Trull T. The natural iron fertilization experiment KEOPS (Kerguelen Ocean and Plateau compared Study):an overview. *Deep-Sea Res II* 2008;**55**:559–65.

Blain S, Renaut S, Xing X, *et al.* Instrumented elephant seals reveal the seasonality in chlorophyll and light-mixing regime in the iron-fertilized Southern Ocean. *Geophys Res Lett* 2013;**40**:6368–72.

Boyd PW, Jickells T, Law CS, *et al.* Mesoscale iron enrichment experiments 5 1993–2005: synthesis and future directions. *Science* 2007;**315**:612–7.

Brussaard CPD, Timmermans KR, Uitz J, *et al.* Virioplankton dynamics and virally induced phytoplankton lysis versus microzooplankton grazing southeast of the Kerguelen (Southern Ocean). *Deep-Sea Res II* 2008;**55**:752–65.

Buskey EJ. Behavioral components of feeding selectivity of the heterotrophic dinoflagellate *Protoperidinium pellucidum*. *Mar Ecol Prog Ser* 1997;**153**:77–89.

Calbet A, Saiz E. The ciliate–copepod link in marine ecosystems. *Aquat Microb Ecol* 2005;**38**:157–67.

Carlotti F, Jouandet M-P, Nowaczyk A, *et al.* Mesozooplankton structure and functioning during the onset of the Kerguelen phytoplankton bloom during the KEOPS2 survey. *Biogeosci Discuss* 2015;**12**:2381–427.

Carlotti F, Thibault-Botha D, Nowaczyk A, *et al.* Zooplankton community structure, biomass and role in carbon fluxes during the second half of a phytoplankton bloom in the eastern sector of the Kerguelen Shelf (January–February 2005). *Deep-Sea Res II* 2008;**55**:720–33.

Cavagna AJ, Fripiat F, Elskens M, *et al.* Biological productivity regime and associated N cycling in the vicinity of Kerguelen Island area, Southern Ocean. *BiogeosciDiscuss* 2014;**11**:18073–104.

Christaki U, Lefèvre D, Georges C, *et al.* Microbial food web dynamics during spring phytoplankton blooms in the naturally iron-fertilized Kerguelen area (Southern Ocean). *Biogeosciences* 2014;**11**:6739–53.

Christaki U, Obernosterer I, Van Wambeke F, *et al.* Microbial food web structure in a naturally iron-fertilized area in the Southern Ocean (Kerguelen Plateau). *Deep-Sea Res II* 2008; **55**:706–19.

Christensen-Dalsgaard KK, Fenchel T. Increased filtration efficiency of attached compared to free-swimming flagellates. *Aquat Microb Ecol* 2003;**33**:77–86.

Clarke KR, Gorley RN. *Primer v6: User Manual/Tutorial*. Plymouth: PRIMER-E, 2006.

Closset I, Lasbleiz M, Leblanc K, *et al.* Seasonal evolution of net and regenerated silica production around a natural Fe fertilized area in the Southern Ocean estimated with Si isotopic approaches. *Biogeosciences* 2014;**11**:5827–46.

Díez B, Pedrós-Alió C, Massana R. Study of genetic diversity of eukaryotic picoplankton in different oceanic regions by small-subunit rRNA gene cloning and sequencing. *Appl Environ Microbiol* 2001;**67**:2932–41.

Doherty M, Costas BA, McManus GB, *et al.* Culture-independent assessment of planktonic ciliate diversity in coastal northwest Atlantic waters. *Aquat Microb Ecol* 2007;**48**:141–54.

d'Ovidio F, Della Penna A, Trull TW, *et al.* The biogeochemical structuring role of horizontal stirring: Lagrangian perspectives on iron delivery downstream of the Kerguelen plateau. *Biogeosci Discuss* 2015;**12**:779–814.

Edgar RC. Search and clustering orders of magnitude faster than BLAST. *Bioinformatics* 2010;**26**:2460–1.

Georges C, Monchy S, Genitsaris S, *et al.* Protist community composition during early phytoplankton blooms in the naturally iron-fertilized Kerguelen area (Southern Ocean). *Biogeosciences* 2014;**11**:5847–63.

Grattepanche J-D, Breton E, Brylinski JM, *et al.* Succession of primary producers and micrograzers in a coastal ecosystem dominated by *Phaeocystis globosa* blooms. *J Plankton Res* 2011a;**33**:37–50.

Grattepanche J-D, Vincent D, Breton E, *et al.* Phytoplankton growth and microzooplankton grazing during a spring bloom in the eastern English Channel. *J Exp Mar Biol Ecol* 2011b;**404**:87–97.

Downloaded from http://femsec.oxfordjournals.org/ by guest on October 6, 2016

Guillou L, Bachar D, Audic S, *et al.* The Protist Ribosomal Reference database (PR2): a catalog of unicellular eukaryote small sub-unit rRNA sequences with curated taxonomy. *Nucleic Acid Res* 2013;**41**:597–604.

Hall JA, Safi K. The impact of in situ Fe fertilization on the microbial food web in the Southern Ocean. *Deep-Sea Res II* 2001;**48**:2591–613.

Hansen PJ. Prey size selection, feeding rates and growth dynamics of heterotrophic dinoflagellates with special emphasis on *Gyrodinium spirale*. *Mar Biol* 1992;**114**:327–34.

Henjes J, Assmy P, Klaas C, *et al.* Response of the larger protozooplankton to an iron-induced phytoplankton bloom in the Polar Frontal Zone of the Southern Ocean (EisenEx). *Deep-Sea Res I* 2007;**54**:774–91.

Hoppenrath M, Elbrächter M, Drebes G. *Marine Phytoplankton*. Germany:Kleine Senckenberg-Reibe 49, 2009.

Horner RA, Postel JR, Halsband-Lenk C, *et al.* Winter–spring phytoplankton blooms in Dabob Bay, Washington. *Prog Oceanogr* 2005;**67**:282–313.

Jacobson DM, Anderson DM. Growth and grazing rates of *Protoperidinium hirobis* Abè, a thecate heterotrophic dinoflagellate. *J Plankton Res* 1993;**15**:723–36.

Jeong HJ, Du Yoo Y, Kim JS, *et al.* Growth, feeding and ecological roles of the mixotrophic and heterotrophic dinoflagellates in marine planktonic food webs. *Ocean Sci* 2010; **45**:65–91.

Karayanni H, Christaki U, Van Wambeke F, *et al.* Heterotrophic nanoflagellate and ciliate bacterivorous activity and growth in the northeast Atlantic Ocean: a seasonal mesoscale study. *Aquat Microb Ecol* 2008;**51**:169–81.

Kiørboe T, Tang K, Grossart HP, *et al.* Dynamics of microbial communities on marine snow aggregates: colonization, growth, detachment, and grazing mortality of attached bacteria. *Appl Environ Microbiol* 2003;**69**:3036–47.

Landa M, Blain S, Christaki U, *et al.* Shifts in bacterial community composition associated to increased carbon cycling in a mosaic of phytoplankton blooms in the Southern Ocean. *ISME J* 2015: 1–12, DOI: 10.1038/ismej.2015.105.

Landry MR, Ondrusek ME, Tanner SJ, *et al.* Biological response to iron fertilization in the eastern equatorial Pacific (IronEx II). I. Microplankton community abundances and biomass. *Mar Ecol Prog Ser* 2000;**201**:27–42.

Lasbleiz M, Leblanc K, Blain S, *et al.* Pigments, elemental composition (C, N, P, and Si), and stoichiometry of particulate matter in the naturally iron fertilized region of Kerguelen in the Southern Ocean. *Biogeosciences* 2014; **11**:5931–55.

López-Garcia P, Philippe H, Gail F, *et al.* Autochthonous eukaryotic diversity in hydrothermal sediment and experimental microcolonizers at the Mid-Atlantic Ridge. *Proc Natl Acad Sci USA* 2003;**100**:697–702.

López-Garcia P, Rodriguez-Valera F, Pedrós-Alió C, *et al.* Unexpected diversity of small eukaryotes in deep-sea Antarctic plankton. *Nature* 2001;**409**:603–7.

Malits A, Christaki U, Obernosterer I, *et al.* Enhanced viral production and virus-mediated mortality of bacterioplankton in a natural iron-fertilized bloom event above the Kerguelen Plateau. *Biogeosciences* 2014;**11**:6841–53.

Martin JH, Fitzwater SE. Iron deficiency limits phytoplankton growth in Antarctic waters. *Global Biogeochem Cycles* 1990;**4**: 5–12.

Massana R, Pedrós-Alió C. Unveiling new microbial eukaryotes in the surface ocean. *Curr Opin Microbiol* 2008;**11**:213–8.

Massana R, Pernice M, Bunge JA, *et al.* Sequence diversity and novelty of natural assemblages of picoeukaryotes from the Indian Ocean. *ISME J* 2011;**5**:184–95.

McMinn A, Scot FJ. Dinoflagellates. In: Scott FJ, Marchant HW (eds). *Antarctic Marine Protists*. Australia: ABRS and AAD Publishers, 2005: pp. 202–250.

Mender-Deuer S, Lessard EJ. Carbon to volume relationships for dinoflagellates, diatoms, and other protist plankton. *Limnol Oceanogr* 2000;**45**:569–79.

Monchy S, Grattepanche J-D, Breton E, *et al.* Microplanktonic community structure in a coastal system relative to a phaeocystis bloom inferred from morphological and tag pyrosequencing methods. *PLoS One* 2012;**7**:e39924.

Mongin M, Molina E, Trull TW. Seasonality and scale of the Kerguelen plateau phytoplankton bloom: a remote sensing and modeling analysis of the influence of natural iron fertilization in the Southern Ocean. *Deep-Sea Res II* 2008;**55**: 880–92.

Montagnes DJS, Allen J, Brown L, *et al.* Role of ciliates and other microzooplankton in the Irminger Sea (NW Atlantic Ocean). *Mar Ecol Prog Ser* 2010;**411**:101–15.

Moon-van der Staay SY, Watcher RD, Vaulot D. Oceanic 18S rDNA sequences from picoplankton reveal unsuspected eukaryotic diversity. *Nature* 2001;**409**:607–10.

Neuer S, Cowles TJ. Protist herbivory in the Oregon upwelling system. *Mar Ecol Prog Ser* 1994;**113**:147–62.

Obernosterer I, Christaki U, Lefèvre D, *et al.* Rapid bacterial mineralization of organic carbon produced during a phytoplankton bloom induced by natural iron fertilization in the Southern Ocean. *Deep-Sea Res II* 2008;**55**:777–89.

Oliver JL, Barber RT, Smith WO, Jr, *et al.* The heterotrophic bacterial response during the Southern Ocean Iron Experiment (SOFeX). *Limnol Oceanogr* 2004;**49**:2129–40.

Park YH, Durand I, Kestenare E, *et al.* Polar front around the Kerguelen islands: an up-to-date determination and associated circulation of surface/subsurface water. *J Geophys Res* 2014;**119**:6575–92.

Petz W. Ciliates. In: Scott FJ, Marchant HJ (eds). *Antarctic Marine Protists*. Australia: ABRS and AAD Publishers, 2005, 347–448.

Pierce RW, Turner JT. Ecology of planktonic ciliates in marine food webs. *Rev Aquat Sci* 1992;**6**:139–81.

Planchon F, Ballas D, Cavagna AJ, *et al.* Carbon export in the naturally iron-fertilized Kerguelen area of the Southern Ocean based on the ^{234}Th approach. *Biogeosci Discuss* 2014;**11**:15991–16032.

Pollard R, Salter I, Sanders R, *et al.* Southern Ocean deep-water carbon export enhanced by natural iron fertilization. *Nature* 2009;**457**:577–81.

Poulton AJ, Moore M, Seeyave S, *et al.* Phytoplankton community composition around the Crozet Plateau, with emphasis on diatoms and Phaeocystis. *Deep-Sea Res II* 2007;**54**:2085–2105.

Putland JN. Microzooplankton herbivory and bacterivory in Newfoudland coastal waters during spring, summer and winter. *J Plankton Res* 2000;**22**:253–77.

Putt M, Stoecker DK. An experimentally determined carbon:volume ratio for marine 'oligotrichous' ciliates from estuarine and coastal waters. *Limnol Oceanogr* 1989;**34**:1097–1103.

Quéguiner B. Iron fertilization and the structure of planktonic communities in high nutrient regions of the Southern Ocean. *Deep-Sea Res II* 2013;**90**:43–54.

Downloaded from http://femsec.oxfordjournals.org/ by guest on October 6, 2016

Quéroué F, Sarthou G, Planquette HF, *et al*. High variability of dissolved iron concentrations in the vicinity of Kerguelen Island (Southern Ocean). *Biogeosci Discuss* 2015;**12**:231–70.

Reeder J, Knight R. The 'rare biosphere': a reality check. *Nat Methods* 2009;**6**:636–7.

Sackett O, Armand L, Beardall J, *et al*. Taxon-specific responses of Southern Ocean diatoms to Fe enrichment revealed by synchrotron radiation FTIR microspectroscopy. *Biogeosciences* 2014;**11**:5795–808.

Saito H, Suzuki K, Hinuma A, *et al*. Responses of microzooplankton to in situ iron fertilization in the Western Subarctic Pacific (SEEDS). *Prog Oceanogr* 2005;**64**:223–36.

Sarthou G, Timmermans KR, Blain S, *et al*. Growth physiology and fate of diatoms in the ocean: a review. *J Sea Res* 2005;**53**:25–42.

Savin MC, Martin JL, LeGresley M, *et al*. Plankton diversity in the bay of Fundy as measured by morphological and molecular methods. *Microb Ecol* 2004;**48**:51–65.

Savoye N, Trull TW, Jacquet SHM, *et al*. ^{234}Th-based export fluxes during a natural iron fertilization experiment in the Southern Ocean (KEOPS). *Deep-Sea Res II* 2008;**55**:841–55.

Schloss PD, Gevers D, Westcott SL. Reducing the effects of PCR amplification and sequencing artifacts on 16S rRNA-based studies. *PLoS One* 2011;**6**:e27310.

Schloss PD, Westcott SL, Ryabin T, *et al*. Introducing mothur: open-source, platform-independent, community-supported software for de-scribing and comparing microbial communities. *Appl Environ Microbiol* 2009;**75**:7537–41.

Sherr EB, Sherr BF. Heterotrophic dinoflagellates: a significant component of microzooplankton biomass and major grazers of diatoms in the sea. *Mar Ecol Prog Ser* 2007;**352**:187–97.

Sherr EB, Sherr BF. Capacity of herbivorous protists to control initiation and development of mass phytoplankton blooms. *Aquat Microb Ecol* 2009;**57**:253–62.

Sherr EB, Sherr BF, McDaniel J. Clearance rates of <6 μm fluorescently labeled algae (FLA) by estuarine protozoa: potential grazing impact of flagellates and ciliates. *Mar Ecol Prog Ser* 1991;**69**:81–92.

Skovgaard A, Massana R, Balagué V, *et al*. Phylogenetic position of the copepod-infesting parasite *Syndinium turbo* (Dinoflagellata, Syndinea). *Protist* 2005;**156**:413–23.

Smetacek VS. Role of sinking in diatom life-history cycles: ecological, evolutionary and geological significance. *Mar Biol* 1985;**84**:239–51.

Smetacek V, Klaas C, Strass VH, *et al*. Deep carbon export from a Southern Ocean iron-fertilized diatom bloom. *Nature* 2012;**487**:313–9.

Stoecker DK, Capuzzo JM. Predation on protozoa: its importance to zooplankton. *J Plankton Res* 1990;**12**:891–908.

Straile D. Gross growth efficiencies of protozoan and metazoan zooplankton and their dependence on food concentration, predator–prey weight ratio, and taxonomic group. *Limnol Oceanogr* 1997;**42**:1375–85.

Strom SL. Growth and grazing rates of the herbivorous dinoflagellate *Gymnodinium* sp. from the open subarctic Pacific Ocean. *Mar Ecol Prog Ser* 1991;**78**:103–13.

Strom SL. Novel interactions between phytoplankton and microzooplankton: their influence on the coupling between growth and grazing rates in the sea. *Hydrobiologia* 2002;**480**:41–54.

Strom SL, Fredrickson KA. Intense stratification leads to phytoplankton nutrient limitation and reduced microzooplankton grazing in the southeastern Bering Sea. *Deep-Sea Res II* 2008;**55**:1761–74.

Strom SL, Strom MW. Microplankton growth, grazing, and community structure in the northern Gulf of Mexico. *Mar Ecol Prog Ser* 1996;**130**:229–40.

Takahashi T, Sutherland SC, Sweeney C, *et al*. Global sea–air CO2 flux based on climatological surface ocean pCO2, and seasonal biological and temperature effects. *Deep-Sea Res II* 2002;**49**:1601–22.

Tomas CR. *Identifying Marine Phytoplankton*. London: Academic Press, 1997.

Uitz J, Claustre H, Griffiths FB, *et al*. A phytoplankton class-specific primary production model applied to the Kerguelen Islands region (Southern Ocean). *Deep-Sea Res I* 2009;**56**:541–60.

Verity PG, Stoecker DK, Sieracki ME, *et al*. Grazing, growth and mortality of microzooplankton during the 1989 North Atlantic spring bloom at 47° N, 18°W. *Deep-Sea Res I* 1993;**40**:1793–1814.

Zeldis J. Mesozooplankton community composition, feeding, and export production during SOIREE. *Deep-Sea Res II* 2001;**48**:2615–34.

Downloaded from http://femsec.oxfordjournals.org/ by guest on October 6, 2016